

# UC Berkeley

## UC Berkeley Previously Published Works

### Title

Levels in Cd125 populated by the  $\beta$  decay of Ag125m and Ag125

### Permalink

<https://escholarship.org/uc/item/4zw2z9qd>

### Journal

Physical Review C, 104(2)

### ISSN

2469-9985

### Authors

Batchelder, JC

Apgar, C

Brewer, NT

et al.

### Publication Date

2021-08-01

### DOI

10.1103/physrevc.104.024308

Peer reviewed

Levels in  $^{125}\text{Cd}$  populated by the  $\beta$  decay of  $^{125m}\text{Ag}$  and  $^{125}\text{Ag}$ 

J. C. Batchelder<sup>1</sup>, C. Apgar<sup>1</sup>, N. T. Brewer<sup>2,3</sup>, C. J. Gross<sup>2</sup>, R. K. Grzywacz<sup>2,4,5</sup>, S. Ilyushkin<sup>6</sup>, M. Madurga<sup>4</sup>, K. Miernik<sup>2,7</sup>, S. W. Padgett<sup>4</sup>, S. V. Paulauskas<sup>4</sup>, W. A. Peters<sup>8</sup>, B. C. Rasco<sup>2,4,5</sup>, K. P. Rykaczewski<sup>2</sup>, D. W. Stracener<sup>2</sup>, J. A. Winger<sup>6</sup>, M. Wolińska-Cichocka<sup>2,5,9</sup>, E. F. Zganjar<sup>10</sup>, D. W. Bardayan<sup>11</sup>, M. E. Howard<sup>12</sup>, B. Manning<sup>12</sup>, M. Matos<sup>2</sup>, A. J. Mendez<sup>2</sup>, D. Miller<sup>4</sup>, A. Ratkiewicz<sup>12</sup> and E. H. Wang<sup>3</sup>

<sup>1</sup>Department of Nuclear Engineering, University of California, Berkeley, Berkeley California 94720, USA

<sup>2</sup>Physics Division, Oak Ridge National Laboratory, Oak Ridge Tennessee 37931, USA

<sup>3</sup>Department of Physics, Vanderbilt University, Nashville Tennessee 37235, USA

<sup>4</sup>Department of Physics, University of Tennessee, Knoxville Tennessee 37996, USA

<sup>5</sup>Joint Institute for Nuclear Physics and Applications, Oak Ridge Tennessee 37831, USA

<sup>6</sup>Department of Physics and Astronomy, Mississippi State University, Mississippi State, Mississippi 39762, USA

<sup>7</sup>Faculty of Physics, University of Warsaw, Warsaw PL-02-093, Poland

<sup>8</sup>Oak Ridge Associated Universities, Oak Ridge, Tennessee 37831, USA

<sup>9</sup>Heavy Ion Laboratory, University of Warsaw, Warsaw, PL 02-093, Poland

<sup>10</sup>Louisiana State University, Baton Rouge, Louisiana 70803, USA

<sup>11</sup>Department of Physics, University of Notre Dame, Notre Dame, Indiana 46556, USA

<sup>12</sup>Department of Physics and Astronomy, Rutgers University, New Brunswick, New Jersey 08901, USA



(Received 25 August 2020; revised 4 May 2021; accepted 6 July 2021; published 4 August 2021)

The  $\beta$  decay of  $^{125m,125}\text{Ag}$  into levels in  $^{125}\text{Cd}$  was investigated at the Holifield Radioactive Ion Beam Facility (HRIBF). Uranium-238 targets were bombarded with 50-MeV protons with an intensity of 15  $\mu\text{A}$ , and the induced fission products were mass separated and deposited on a moving tape in the center of the VANDLE array consisting of  $\gamma$  detectors and plastic scintillators. A partial decay scheme has been assigned for both  $\beta$  decay of the  $(9/2^+)$  ground state of  $^{125}\text{Ag}$  and its low-lying  $(1/2^-)$  isomer, with the energy of the low-lying  $(11/2^-)$  isomeric state in  $^{125}\text{Cd}$  assigned as 188.5 keV. In addition,  $\beta$ -delayed neutron emission probabilities were also determined to be 1.2(2)% for the  $(9/2^+)$   $^{125}\text{Ag}$  ground state and 4.6(10)% for the  $(1/2^-)$  isomer, which are substantially lower than the previously reported value.

DOI: [10.1103/PhysRevC.104.024308](https://doi.org/10.1103/PhysRevC.104.024308)

## I. INTRODUCTION

In the region of the Segre chart near the doubly magic nucleus  $^{132}\text{Sn}$  there is an abundance of long-lived isomeric states. This is largely due to low-lying  $\pi g_{9/2}$  and  $\nu h_{11/2}$  configurations near several low- $j$  orbitals. One of the best systems to pursue such studies is that of neutron-rich cadmium nuclei because they are near the closed proton and neutron shells at  $Z = 50$  and  $N = 82$ , respectively. The odd- $A$  isotopes of cadmium, near  $N = 82$  in particular, are all known to exhibit low-energy isomers with half-lives similar to those of their ground states. A systematic study of these levels allows one to map the single-particle states of these and nearby configurations across the chart. For nuclei that are far from stability,  $\beta$  decay is the best way to populate these low-energy and low-spin levels. For the cases of odd-mass Ag and Cd isotopes, the study of the  $\beta$  decay of these nuclei and their isomers gives information on the  $\pi 1g_{9/2}$  and  $\pi 2p_{1/2}$  states in Ag and the  $\nu 1h_{11/2}$  and  $\nu 2d_{3/2}$  states in Cd, and the levels built on them.

On the neutron-rich side of stability, the levels of odd-mass Ag isotopes from  $^{111}\text{Ag}$  to  $^{123}\text{Ag}$  [1–7] have been extensively measured via the  $\beta$  decay of Pd isotopes. In all these cases,

long-lived isomers were observed in the Ag isotopes. The spins and parities of the ground state of  $^{111}\text{Ag}$  and  $^{113}\text{Ag}$  have been measured via atomic beam as  $1/2^-$  [8] with the isomer assigned as  $7/2^+$  based on the  $\beta$ - and  $\gamma$ -decay patterns. Silver-115 and  $^{117}\text{Ag}$  have been assigned as  $(1/2^-)$  for the ground state and  $(7/2^+)$  for the isomeric levels based on the systematics of these lighter Ag isotopes [3,4]. The energy of the  $1/2^-$  and  $7/2^+$  levels were reported to have been reversed in  $^{119}\text{Ag}$  based on the  $\beta$ -decay pattern of  $^{119}\text{Pd}$  [9] with the  $(7/2^+)$  level as the ground state. As such, the ground states of  $^{121,123}\text{Ag}$  have also been assigned  $(7/2^+)$  based on systematics.

For levels in the Cd isotopes,  $\beta$ -decay studies of odd-mass Ag isotopes have identified levels in Cd up to  $^{123}\text{Cd}$  [6,10] including a long-lived 1.81(3) s  $(11/2^-)$  isomer whose excitation energy was assigned as 316.4 keV based on decay pattern and systematics. A later study by Kankainen *et al.* involving the JYFLTRAP [11] assigned a value of 144(4) keV to the excitation of the isomer. For the case of  $^{125}\text{Cd}$ , a long-lived isomer was observed with a half-life of 0.48(3) s by Huck *et al.* [10] and the excitation energy measured via JYFLTRAP [11] as 186(5) keV and 190(26) keV in the TITAN experiment at TRIUMF [12]. In addition, long-lived isomers have also

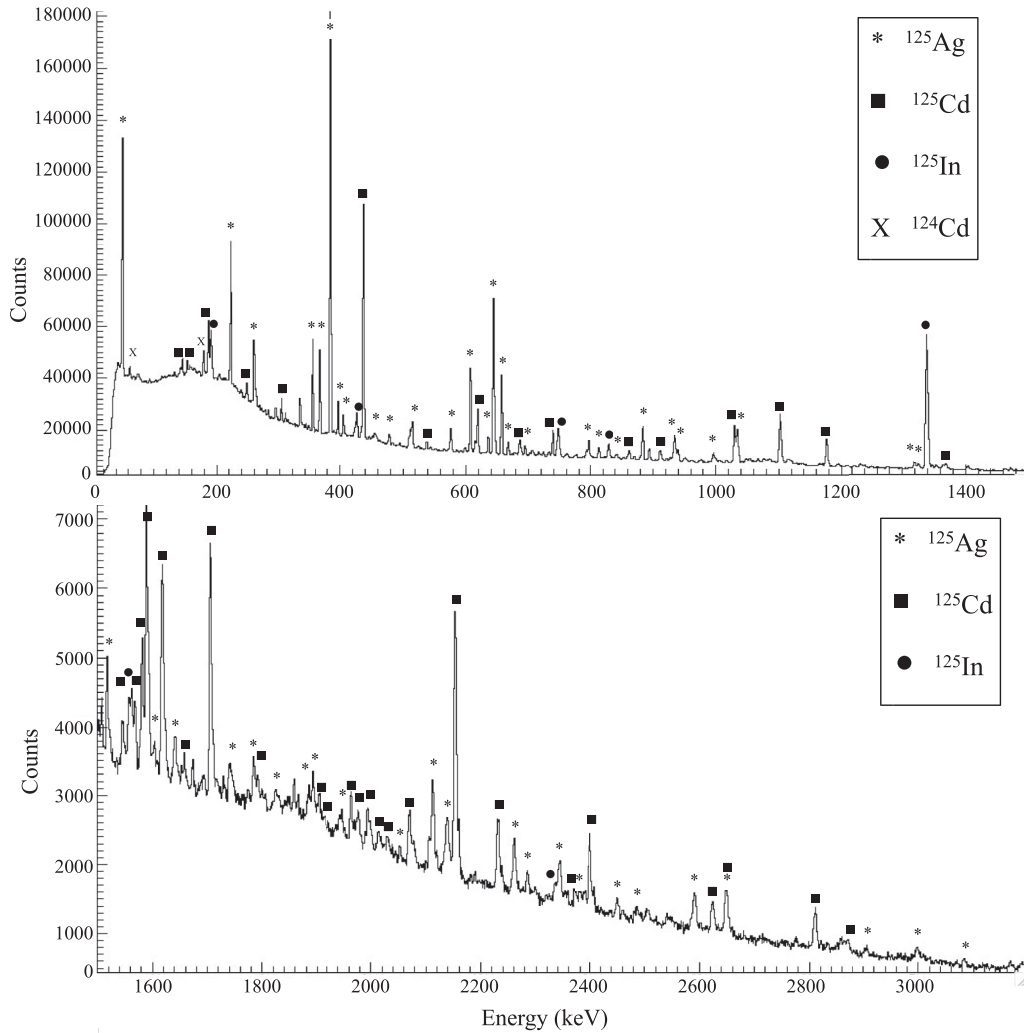


FIG. 1. Total mass  $^{125}\gamma$  spectrum gated on the  $\beta$  detectors. In this figure, known  $\gamma$  rays from  $^{124,125}\text{Cd}$ ,  $^{125}\text{In}$  are labeled along with  $\gamma$ s that we assign to the  $\beta$  decay of  $^{125}\text{Ag}$ . For the cases where peaks have unresolved contribution from more than one isotope, the major isotope is labeled.

been observed in  $^{127}\text{Cd}$  [13,14] and  $^{129}\text{Cd}$  [15]. In neither of these two cases has the relative isomer excitation been established.

Other information on levels in  $^{125}\text{Cd}$  comes from thermal-neutron-induced fission studies of  $^{239}\text{Pu}$  [16,17] and fragmentation of a  $^{136}\text{Xe}$  and passed through a separator [13]. In these studies, high spin ( $\geq 15/2$ ) states are observed to feed the  $11/2^-$  isomer. These states would not be expected to be populated in  $\beta$  decay due to the large change in angular momentum. Fragmentation studies of  $^{238}\text{U}$  by Rejmund *et al.* [18] observed the previously known  $743\gamma$  feeding the  $11/2^-$  isomer of  $^{125}\text{Cd}$ , and 233, 250, 570, 646, 663, 756, and 844 keV  $\gamma$ s, which may be positive-parity yrast transitions feeding the  $3/2^+$  ground state of  $^{125}\text{Cd}$ , of which the lower spin states could be populated in the  $\beta$  decay of  $^{125}\text{Ag}$ .

Information on the  $\beta$  decay of  $^{125}\text{Ag}$  and the resulting populated levels in  $^{125}\text{Cd}$  is very limited. The half-life of  $^{125}\text{Ag}$  has been measured via the delayed neutron curve as

$166(7)$  ms [19],  $163^{+9}_0$  ms [20],  $146(11)$  ms [21], also via an ion-implanted decay curve as  $150(8)$  ms [22]. A  $\beta$ -decaying isomer of  $^{125}\text{Ag}$  was observed at 97.1 keV in the  $\beta$  decay of  $^{125}\text{Pd}$  [23]. The  $J^\pi$  of the ground state was assigned as  $(9/2^+)$  and the isomer as  $(1/2^-)$  based on the decay pattern of  $^{125}\text{Pd}$  and shell-model calculations performed using the KSHELL code with a monopole-based universal interaction plus a spin-orbit force [23]. This work also reported  $\gamma$  rays of 383.6 and 643.2 keV assigned as  $\gamma$ s that feed the ground-state decay of  $^{125}\text{Cd}$ , along with  $\gamma$  rays of 352.7, 383.6, and 643.2 keV assigned as  $\gamma$ s that feed the isomer of  $^{125}\text{Cd}$ . These  $\gamma$  rays were not assigned to a decay scheme and no uncertainties were assigned to the energies in this work. The mass of  $^{125}\text{Ag}$  has been measured the Fragment Separator (FRS) at GSI [11] resulting in  $Q_\beta = 8830(430)$  and  $Q_{\beta n} = 4110(430)$  [24]. The currently known levels in  $^{125}\text{Cd}$  are limited to an  $11/2^-$  isomer and a high spin band built on the  $11/2^-$  isomer [13,25], whose levels would not be expected to be populated in the  $\beta$  decay of  $^{125}\text{Ag}$ .

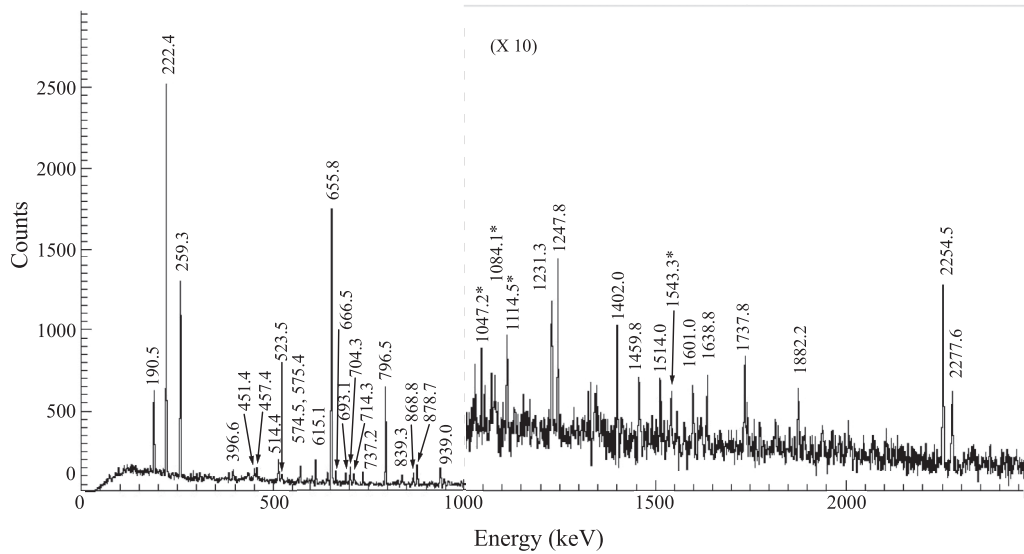


FIG. 2.  $\beta$ -gated  $\gamma$ -ray spectrum coincident with the 384.1-keV transition. The energies of prominent  $\gamma$  peaks are labeled. Those transitions that are not included in the proposed decay scheme are labeled with \*.

Measurement of the  $\beta$ -delayed neutron branch also provides insight into nuclear structure above the neutron separation energy of nuclei near doubly closed  $^{132}\text{Sn}$  and the  $A = 130$   $r$ -process abundance peak and is vitally important to the understanding of the astrophysical  $r$  process. Significant  $\beta$ -delayed neutron emission can potentially affect the final abundances of nuclei produced in this process. Although  $^{125}\text{Ag}$  is not directly on the  $r$  process path, knowledge of its  $\beta$ - $n$  branching ratio can provide information with which to evaluate astrophysical  $r$ -process network calculations. The  $\beta$ - $n$  branching ratio for  $^{125}\text{Ag}$  has been reported as 11.8(10)% in an unpublished thesis [20] and more recently in Ref. [21] as 2.2(11)%, without distinguishing between the ground state and isomeric decays in either work.

## II. EXPERIMENTAL METHOD

Fission products were produced via the proton-induced fission of  $^{238}\text{U}$  at the Holifield Radioactive Ion Beam Facility (HRIBF). Fifty MeV protons with an intensity of  $\approx 15 \mu\text{A}$  from the ORIC cyclotron were used to bombard a  $^{238}\text{U}$  target [26] in a plasma ion source installed at the IRIS-2 [27]. The proton-induced fission products were then mass-separated via a high-resolution ( $\Delta m/m \approx 10\,000$ ) magnet and delivered to the VANDLE (the Versatile Array of Neutron Detectors at Low Energy) detector array, where they were embedded on a tape located in the center of the array [28]. The array consisted of two high-purity Ge (HPGe) clover detectors which measured  $\gamma$  transitions, two plastic scintillators surrounding the collection spot for detection of  $\beta$  particles, and

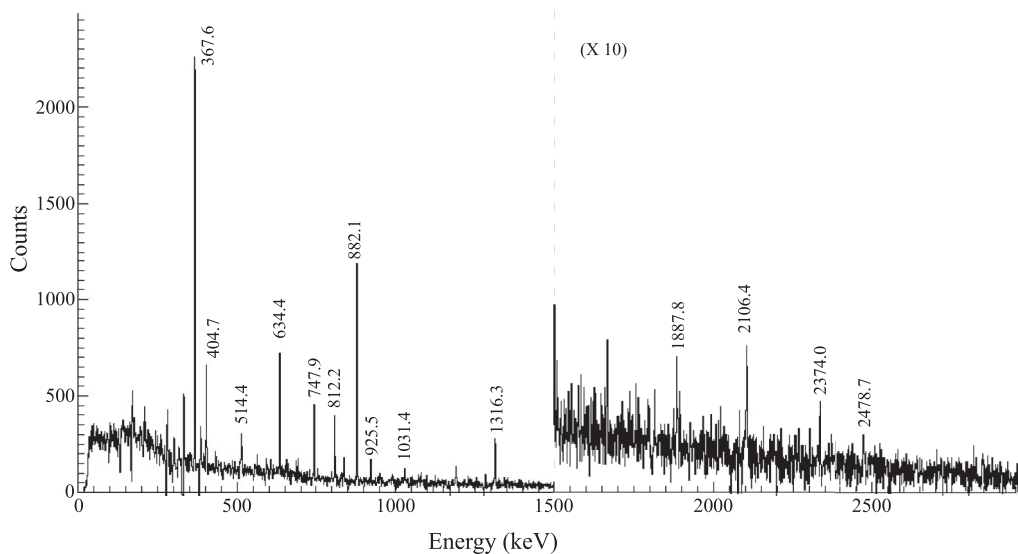


FIG. 3.  $\beta$ -gated  $\gamma$ -ray spectrum coincident with the 50.5-keV transition. Prominent  $\gamma$  peaks that are included in our proposed decay scheme of  $^{125}\text{Ag}$  are labeled.

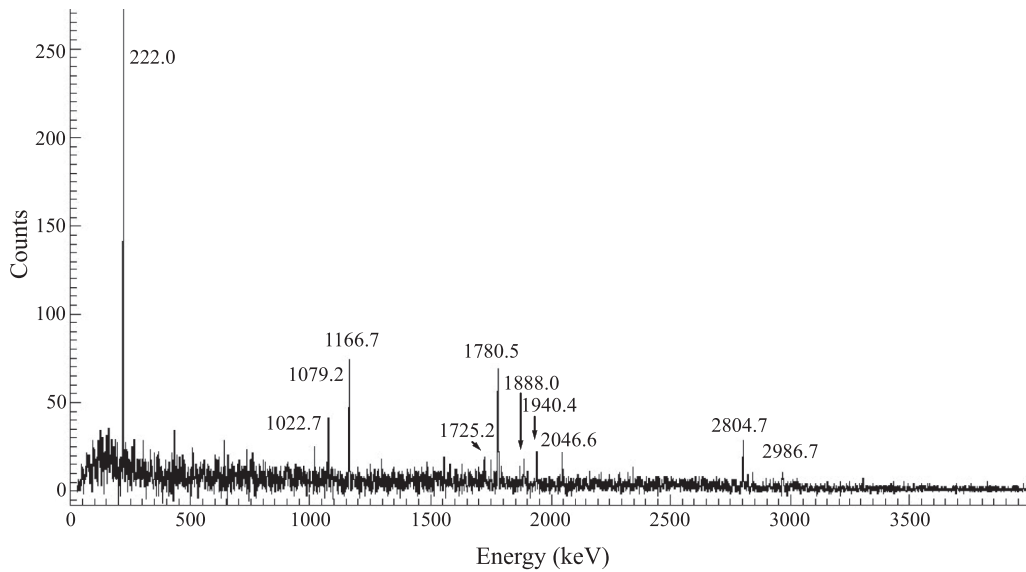


FIG. 4.  $\beta$ -gated  $\gamma$ -ray coincident with the 352.6-keV transition. Prominent  $\gamma$  peaks that are included in our proposed decay scheme of  $^{125m}\text{Ag}$  are labeled.

48 plastic scintillators for detection of neutron energies via their time of flight between the two scintillators surrounding the beam spot and the scintillators at a distance of 50 cm. The clover detector’s photopeak efficiency was  $\approx 4\%$  at 1.33 MeV. The results contained herein were obtained from  $\gamma$ -ray information, while information obtained from the neutron array will be presented in the future.

The beam of mass 125 was pulsed via electrostatic plates with the beam on for the first 2 s, and then turned off for 0.5 s for a total of 2.5 s to allow the half-life measurements. This resulted in a 2 s grow-in, followed by 0.5 s decay cycle, during which the ion beam was deflected away by the electrostatic plates. Afterwards, the tape moved the collected radioactivity to a Pb-shielded area 50 cm away from the collection spot.

Coincidences between the HPGe detectors and the scintillators (which were shaped to surround the beam-line) allowed us to remove the vast majority of  $\gamma$  rays from either the room or longer-lived daughter products on the used tape. The tape cycle time was chosen to enhance the observation of the short-lived  $^{125}\text{Ag}$  nucleus. Cadmium-125 and  $^{125}\text{In}$  are present in this data set both from being deposited on the tape directly and as the  $\beta$ -daughter products. The direct production rate of  $^{125}\text{Cd}$  and  $^{125}\text{In}$  from  $^{238}\text{U}$  fission are orders of magnitude higher than Ag. With no isobaric separation or tape movement, the ratio Ag : Cd : In was expected to be [29]  $\approx 1 : 70 : 650$  for mass 125.

The short tape cycle compared with the half-lives of the Cd and In isomers greatly favors the decays of Ag, however,

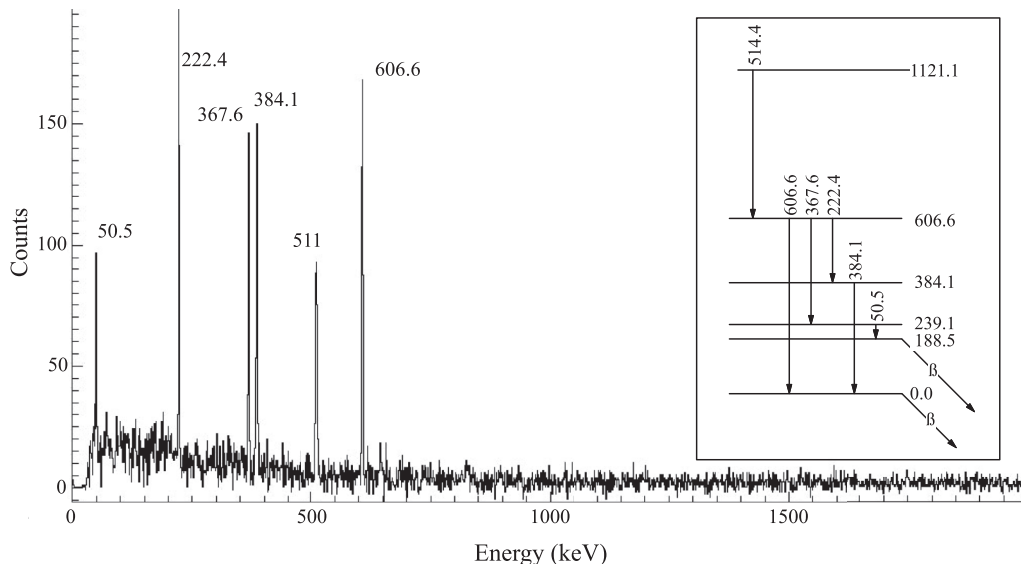


FIG. 5.  $\beta$ -gated  $\gamma$ -ray spectrum in coincidence with the 514.4-keV transition.

TABLE I. List of  $\gamma$  rays resulting from the beta decay of ground state of  $^{125}\text{Ag}$  to levels in  $^{125}\text{Cd}$ . The intensities in columns two and four are normalized to the 100% 384-keV transition. The  $I_{\text{tot}}$  intensities in column four are the total transition strength ( $I_{\gamma} + I_{\text{conversion electron}}$ ).  $\gamma$  intensities are based on (a) singles, or (b) coincidence relationships. The \* symbol means that  $\gamma$  is not in the level scheme. Contaminants from the  $\beta$  decay of  $^{125}\text{Cd}$  are marked with the symbol \*\*, and  $^{125}\text{In}$  with \*\*\*.

$E_{\gamma}$ (keV)	$I_{\gamma}$ (%)	$\alpha_{\text{tot}}$	$I_{\text{tot}}$ (%)	$E_i$	$E_f$	Mult.	Coincident $\gamma$ rays
50.5(1)	17.1(3) <sup>a</sup>	3.30	72.5(12)	239.0	188.5	(M1)	368, 405, 514, 564, 634, 748, 812, 841 882, 926, 1031, 1316, 1654*, 1888 2106, 2374, 2479
222.4(2)	16.3(4) <sup>b</sup>		17.6(5)	606.6	384.1		384, 514, 693
259.3(2)	9.0(10) <sup>b</sup>	0.044	8.8(10)	643.7	384.1	(M1, E2)	384, 397, 455, 478, 656
292.7(3)	1.3(4) <sup>b</sup>		1.3(4)	1615.4	1322.7		384, 1323
309.1(2)	1.4(4) <sup>b</sup>		1.4(4)	1632.0	1322.7		384, 939, 1323
334.0(6)*	0.30(15) <sup>b</sup>		0.30(15)				191, 574
367.6(2)	16.4(10) <sup>b</sup>		16.2(10)	606.6	239.0		51, 514, 693, 949, 1031
384.1(1)	100 <sup>a</sup>	0.0041	100	384.1	0.0	(E1)	191, 222, 259, 293, 397, 451, 457 514, 524, 575, 615, 656, 667, 693, 704 714, 737, 797, 839, 869, 879, 939, 960 994, 1042*, 1084*, 1115*, 1231, 1248 1404, 1460, 1543*, 1601 1639, 1738 1819, 1882, 1941*, 2255, 2278 2643, 2843, 2897, 2999, 3074
396.6(3)	6.4(4) <sup>b</sup>		6.3(4)	1040.0	643.7		259, 384, 405, 575, 644, 704, 714
404.7(3)	4.6(6) <sup>b</sup>	0.004	4.5(6)	643.7	239.0	(E1)	51, 397, 656
451.4(2)	1.2(4) <sup>b</sup>		1.2(4)	1632.0	1180.8		384, 797
454.8(3)	1.9(5) <sup>a</sup>		1.9(5)	1754.3	1299.7		259, 384, 607, 644, 656, 693
457.4(3)	1.3(4) <sup>a</sup>		1.3(4)	1638.0	1180.8		384, 797
477.5(2)	2.5(5) <sup>b</sup>		2.5(5)	1121.1	643.7		259, 384, 644
514.4(4)	10.7(27) <sup>a</sup>		10.7(27)	1121.1	606.6		51, 222, 368, 384, 607
523.5(4)	0.58(12) <sup>b</sup>		0.57(12)	907.6	384.1		384
537.1(4)	1.3(2) <sup>b</sup>		1.3(2)	1180.8	643.7		644
563.7(5)	0.6(4) <sup>a</sup>		0.6(4)	1550.7	986.9		51, 748
574.5(2)	3.2(9) <sup>b</sup>		3.1(9)	1180.8	606.6		222, 334*, 384, 607, 1558*
575.4(2)	1.6(3) <sup>b</sup>		9.1(18)	1615.4	1040.0		384, 397, 656, 1057*
606.6(1)	32.8(5) <sup>a</sup>		32.4(5)	606.6	0.0		191**, 455, 514, 575, 693, 948, 1031, 1514
615.1(4)	1.9(3) <sup>b</sup>		1.9(3)	999.2	384.1		384
634.4(3)	5.9(5) <sup>b</sup>		5.8(5)	873.5	239.0		51
643.8(2)	87.9(25) <sup>a</sup>	0.003	86.8(24)	643.7	0.0	(E2)	398, 478, 537, 656, 912, 994, 1163*, 1477
655.8(2)	24.3(8) <sup>b</sup>		24.0(8)	1040.0	384.1		384
655.9(2)	5.7(6) <sup>b</sup>		5.7(6)	1299.7	643.7		259, 384, 405, 455, 575, 644, 704, 714, 960
666.5(3)	0.66(21) <sup>b</sup>		0.65(21)	1050.6	384.1		384
693.1(4)	4.6(12) <sup>b</sup>		4.6(12)	1299.7	606.6		51, 222, 368, 384, 607
704.3(3)	1.5(3) <sup>b</sup>		1.5(3)	1744.3	1040.0		384, 297, 656
714.3(4)	1.2(3) <sup>b</sup>		1.2(3)	1754.3	1040.0		384, 398, 656
737.2(4)	1.1(2) <sup>b</sup>		1.1(2)	1121.1	384.1		146**, 191**, 384, 722**, 730** 910**, 1173**
747.9(3)	4.9(5) <sup>b</sup>		4.9(5)	986.9	239.0		51
796.5(2)	8.9(6) <sup>b</sup>		8.7(6)	1180.8	384.1		384, 451, 457, 1402, 1460
812.2(3)	4.2(8) <sup>b</sup>		4.2(8)	1051.2	239.0		51
839.3(2)	1.2(2) <sup>b</sup>		1.2(2)	1223.4	384.1		384
868.8(4)	1.4(3) <sup>b</sup>		1.4(3)	1908.8	1040.0		384, 397, 644, 656
878.7(3)	2.1(2) <sup>b</sup>		2.1(2)	1262.8	384.1		384
882.1(2)	20.0(19) <sup>b</sup>		19.8(19)	1121.1	239.0		51
912.0(2)	2.5(5) <sup>b</sup>		2.5(5)	1555.5	643.7		644
925.5(3)	2.7(7) <sup>b</sup>		2.7(7)	1164.3	239.0		51
932.5(2)	18.2(4) <sup>a</sup>		17.9(4)	1121.1	188.5		1888
939.0(2)	1.8(3) <sup>b</sup>		1.8(3)	1322.7	384.1		384
948.9(3)	3.9(10) <sup>b</sup>		3.9(10)	1555.5	606.6		368, 607
960.2(3)	0.47(17) <sup>b</sup>		0.53(19)	2000.2	1040.0		384, 656
975.5(5)	1.4(2) <sup>a</sup>		1.4(2)	1164.3	188.5		

TABLE I. (*Continued.*)

$E_\gamma$ (keV)	$I_\gamma$ (%)	$\alpha_{\text{tot}}$	$I_{\text{tot}}$ (%)	$E_i$	$E_f$	Mult.	Coincident $\gamma$ rays
994.2(2)	4.3(5) <sup>b</sup>		4.3(5)	1638.0	643.7		384, 644
1031.4(2)	3.6(10) <sup>b</sup>		3.5(10)	1638.0	606.6		51, 222, 368, 384, 607
1057.2(5)*	0.4(2) <sup>a</sup>		0.4(2)				384, 575
1084.1(5)*	0.8(2) <sup>b</sup>		0.8(2)				384
1114.5(5)*	0.8(2) <sup>b</sup>		0.8(2)				384
1163.0(5)*	2.6(7) <sup>b</sup>		2.6(7)				384
1231.3(2)	1.5(3) <sup>b</sup>		1.7(3)	1615.4	384.1		384
1247.8(2)	1.9(3) <sup>b</sup>		1.9(3)	1632.0	384.1		384
1316.3(2)	5.9(11) <sup>b</sup>		5.8(11)	1555.5	239.0		51
1322.8(2)	4.4(3) <sup>a</sup>		4.4(3)	1322.9	0.0		293, 309
1402.2(3)	3.3(6) <sup>b</sup>		3.2(6)	2583.0	1180.8		384, 797
1459.8(3)	2.5(5) <sup>b</sup>		2.5(5)	2640.5	1180.8		384, 797
1476.5(3)	2.0(4) <sup>b</sup>		2.0(4)	2120.4	643.7		644
1514.0(5)	1.1(4) <sup>b</sup>		1.1(4)	2120.4	606.6		607
1543.3(5)*	1.1(3) <sup>b</sup>		1.1(4)				384
1558.1(4)*	0.7(4) <sup>b</sup>		0.7(4)				384, 574, 618***
1601.0(5)	1.6(3) <sup>b</sup>		1.6(3)	1985.1	384.1		384
1638.8(4)	1.6(3) <sup>b</sup>		1.6(3)	2022.9	384.1		384
1654.2(4)*	1.4(5) <sup>b</sup>		1.6(3)				50
1737.8(5)	1.7(3) <sup>b</sup>		1.7(3)	2121.9	384.1		384
1818.5(5)	0.57(16) <sup>b</sup>		0.56(16)	2202.6	384.1		384
1882.2(5)	1.1(3) <sup>b</sup>		1.1(3)	2266.3	384.1		384
1887.8(5)	3.4(11) <sup>b</sup>		3.4(11)	3008.9	1121.1		51, 882
1940.6(5)	0.9(3) <sup>b</sup>		0.9(3)				384
2106.4(5)	9.4(5) <sup>b</sup>		9.3(5)	3227.5	1121.1		51, 607, 882, 933
2254.5(3)	6.4(4) <sup>b</sup>		6.4(4)	2638.6	384.1		384
2277.6(3)	2.9(3) <sup>b</sup>		2.9(3)	2661.7	384.1		384
2336.8(5)	5.6(7) <sup>a</sup>		5.6(7)	2980.6	643.7		644
2374.0(5)	7.0(18) <sup>b</sup>		6.9(18)	2980.6	606.6		51, 222, 368, 384, 607
2478.7(5)	3.1(10) <sup>b</sup>		3.1(10)	3085.3	606.6		51, 222, 368, 384, 607
2534.0(5)	3.2(11) <sup>b</sup>		3.1(11)	3140.6	606.6		222, 368, 384, 607
2583.7(5)	8.9(9) <sup>b</sup>		8.8(9)	3227.5	643.7		644
2642.7(5)	5.2(15) <sup>b</sup>		5.1(15)	3249.3	606.6		51, 222, 368, 384, 607
2843.0(4)	1.6(3) <sup>b</sup>		1.6(3)	3227.5	384.1		384
2897.2(4)	2.0(4) <sup>b</sup>		2.0(4)	3281.3	384.1		384
2999.2(4)	1.1(3) <sup>b</sup>		1.1(3)	3383.3	384.1		384
3074.0(4)	1.1(3) <sup>b</sup>		1.1(3)	3458.1	384.1		384

this will only improve the ratio to  $\approx 1 : 23 : 63$ . After tuning the high-resolution magnet to sufficiently enhance the  $\gamma$  rays resulting from the decay of Ag compared with Cd and In, the resulting efficiency-corrected measured ratios (running at the short tape cycle) for  $^{125}\text{Ag} : ^{125}\text{Cd} : ^{125}\text{In}$  was  $\approx 1 : 1.1 : 1.7$ . The other members of the isobaric chain (Pd, Rh) are refractory metals, which have a very low efficiency for release from the ion source and are not observed. The only other nuclei observed from any other mass results from the  $\beta$ -delayed neutron emission of  $^{125}\text{Ag}$ .

The data-acquisition system made use of a digital spectroscopy system based on XIA Pixie16 Rev. F modules (produced by X-ray Instrumentation Associates) [30]. These modules incorporate 250 MHz flash ADCs and serve as a replacement for amplifiers, discriminators, conventional ADCs and TDCs. All signals from the preamps are connected directly into the PIXIE 16 modules then analyzed via the on-board processors to determine their amplitude by fitting

the waveform, and time-stamped by a continuously running clock.

A 16 ns (four channel) coincidence time gate was used to produce prompt  $\gamma$ - $\gamma$  matrices. A time-delayed matrix gated with the same time width was used to subtract the random background from the prompt  $\gamma$ - $\gamma$  matrices. To calibrate the efficiency of the Ge detectors, standard sources of  $^{133}\text{Ba}$ ,  $^{60}\text{Co}$ , and  $^{152}\text{Eu}$  were used. The relative error in efficiency in the energy range of these isotopes was determined to be 6%. For  $\gamma$  rays above 1.4 MeV, the extrapolated efficiencies were assigned the following errors: 6% for  $E \leq 1.8$  MeV, 10% for  $1.8 \text{ MeV} < E \leq 2.5$  MeV, 15% for  $2.5 \text{ MeV} < E \leq 3.0$  MeV, and 20% for  $E > 3.0$  MeV.

### III. EXPERIMENTAL RESULTS

Transitions have been placed in the decay schemes from information obtained via  $\gamma$ - $\gamma$  and  $\beta$ - $\gamma$ - $\gamma$  coincidences. All

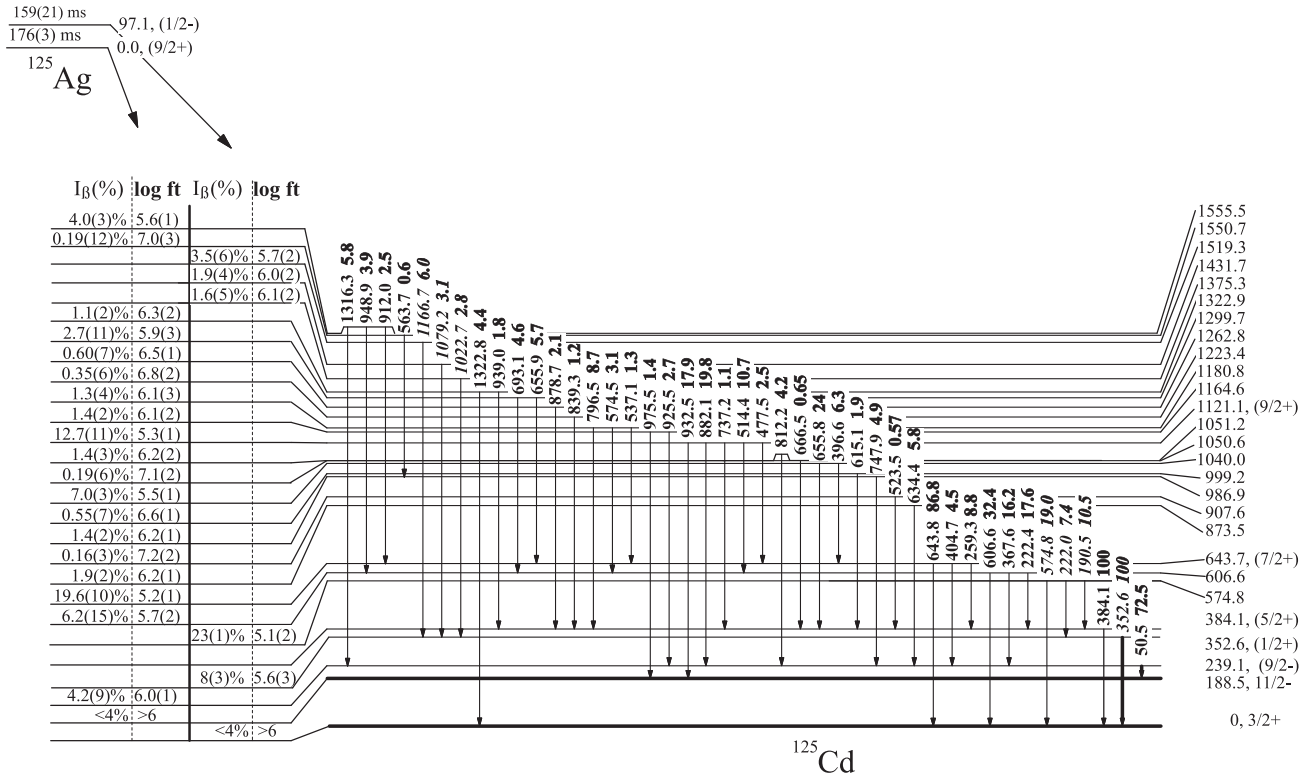


FIG. 6. Proposed partial decay scheme for the  $\beta$  decay of  $^{125}\text{Ag}$  and  $^{125m}\text{Ag}$  (part 1 of 2). For each transition, the energy of the transition is listed in keV, followed by the total intensity ( $\gamma$  plus conversion electron) normalized to the 384.1 keV transition for  $\gamma$  transitions arising from the  $\beta$  decay of the ground state and normalized to the 352 keV transition for  $\gamma$  from the beta decay of the  $1/2^-$  isomer (shown in italics). The ratios of  $\gamma$  transitions deexciting a given state were determined by  $\gamma$ - $\gamma$  coincidences whenever possible.

possible coincidence spectra were analyzed to determine this. The relative intensities of the  $\gamma$  transitions deexciting a given level were determined wherever possible both by coincidences with  $\gamma$  transitions feeding the given level and by gating from below. Gammas that arise from decaying nuclei on the tape from previous cycles and background events will not cause coincidences between the  $\beta$  and  $\gamma$  detectors and can therefore be determined not to arise from  $^{125}\text{Ag}$ .

Figure 1 shows the total  $\gamma$  spectrum gated on the  $\beta$  detectors. In this figure, known  $\gamma$  rays from  $^{125}\text{Cd}$ ,  $^{125}\text{In}$ , along with transitions that we assign to  $\gamma$  transitions resulting from the  $\beta$  decay and  $\beta$ -delayed neutron emission of  $^{125}\text{Ag}$ . The previously reported 352.7, 383.6, and 643.2 keV  $\gamma$ s [23] from  $^{125}\text{Ag}$  are all observed in this work.

Beta decay from the ( $1/2^-$ ) isomer and ( $9/2^+$ ) ground state will feed very different states due to the large difference in spin and opposite parities. One would expect that any levels observed in a given state would only be populated by one of the two  $\beta$ -decaying states. The observed gammas can be placed in two groups via their  $\gamma$ - $\gamma$  coincidences. Group 1 are those  $\gamma$ s in coincidence with either the 384.1 (see Fig. 2) or 50.5 keV  $\gamma$  transitions (see Fig. 3), and group 2 being those in coincidence with the 352.6-keV  $\gamma$  transition (see Fig. 4). The 50.5 and 384.1 keV transitions are connected via feeding from above from several  $\gamma$  rays, the strongest of which is the 514.4 keV transition (see Fig. 5). We propose that these represent  $\beta$  decays from two isomers in  $^{125}\text{Ag}$ : a high-spin

( $9/2^+$ ) ground state and a low-spin ( $1/2^-$ ) isomeric state, with the assignment based on their respective decay to the low-spin  $3/2^+$  and high-spin  $11/2^-$  isomers in  $^{125}\text{Cd}$ . Overall, we have observed a total of 73  $\gamma$  rays from 47 levels that are assigned to the  $\beta$  decay of the ground state of  $^{125}\text{Ag}$  and 17  $\gamma$  rays from 14 levels we assign to the  $\beta$  decay of  $^{125m}\text{Ag}$ .

#### A. Decay of the ( $9/2^+$ ) ground state of $^{125}\text{Ag}$

The observed  $\gamma$ -ray transitions resulting from the  $\beta$  decay of the ( $9/2^+$ ) ground state of  $^{125}\text{Ag}$  are listed in Table I. For  $\gamma$ -transitions with assigned multiplicities the  $K$ -conversion coefficients ( $\sigma_k$ ) are calculated using the conversion coefficient calculator BRICC [31], along with the assigned  $J^\pi$  and energies of their initial and final states. In all cases except for the 50.5 keV  $\gamma$ , these values are relatively small and will not make large changes in the total intensities. The assignment of the multipolarity of the 50.5 keV transition is detailed in the next section. The last column in Table I list the  $\gamma$  rays in coincidence with the given transition. Transitions and levels that require further explanation are listed in the following sections by level.

Table II lists the levels in  $^{125}\text{Cd}$  populated in the  $\beta$  decay of the ( $9/2^+$ ) ground state of  $^{125}\text{Ag}$ . The corresponding assignment of  $J^\pi$  for the low-energy levels is based on the decay pattern of the  $\gamma$  rays deexciting these levels. The calculated  $\log ft$  values are based on the apparent  $\beta$  feeding to the given





TABLE II. Levels in  $^{125}\text{Cd}$  populated by the  $\beta$  decay of the ( $9/2^+$ ) ground state of  $^{125}\text{Ag}$ .

Level (keV)	$\beta$ (%)	$\log ft$
0.0	0	
188.5(2)	<4	>6
239.1(1)	4.2(9)	6.0(1)
384.1(1)	0	
606.6(1)	6.2(15)	5.7(2)
643.7(2)	19.6(10)	5.2(1)
873.5(3)	1.9(2)	6.2(1)
907.6(4)	0.16(3)	7.2(2)
986.9(3)	1.4(2)	6.2(1)
999.2(4)	0.55(7)	6.6(1)
1040.0(2)	7.0(3)	5.5(1)
1050.6(3)	0.19(6)	7.1(2)
1051.2(3)	1.4(3)	6.2(2)
1121.1(3)	12.7(11)	5.3(1)
1164.6(3)	1.4(2)	6.1(2)
1180.8(2)	1.3(4)	6.1(3)
1223.4(2)	0.35(6)	6.8(2)
1262.8(3)	0.60(7)	6.5(1)
1299.7(3)	2.7(11)	5.9(3)
1322.9(2)	1.1(2)	6.3(2)
1550.7(5)	0.19(12)	7.0(3)
1555.5(2)	4.0(3)	5.6(1)
1615.4(2)	1.4(2)	5.9(1)
1632.0(2)	1.4(2)	5.9(2)
1638.0(2)	2.9(3)	5.7(1)
1744.3(3)	0.5(1)	6.5(2)
1754.3(4)	1.0(9)	6.2(4)
1908.8(4)	0.45(10)	6.5(2)
1985.1(5)	0.5(1)	6.4(2)
2000.2(3)	0.15(5)	6.9(2)
2022.9(4)	0.2(1)	6.4(2)
2120.4(3)	0.98(17)	6.3(2)
2121.9(5)	0.5(1)	6.4(2)
2202.6(5)	0.17(5)	6.9(2)
2266.3(5)	0.36(10)	6.5(2)
2583.0(3)	1.0(2)	5.9(2)
2638.6(3)	2.0(1)	5.6(2)
2640.5(3)	0.80(16)	5.7(2)
2661.7(3)	0.91(9)	6.0(2)
2980.6(4)	4.0(6)	5.2(2)
3008.9(5)	1.1(3)	5.5(2)
3085.3(5)	1.0(3)	5.8(2)
3140.6(5)	1.0(4)	5.8(2)
3227.5(5)	6.4(4)	5.0(2)
3249.3(5)	1.7(5)	5.5(2)
3281.3(4)	0.6(1)	5.9(2)
3383.3(4)	0.33(8)	6.2(2)
3458.1(4)	0.35(8)	6.1(2)
>4718	1.2(2)	

level as the expected  $11/2^-$  isomer. A  $\gamma$  emitted from this state to the  $3/2^+$  ground state would have a multipolarity of  $M4$  and would be much slower than the measured  $T_{1/2}$  of 480(30) ms [10] and have a vanishingly small branching ratio.

The 50.5-keV transition feeds a  $11/2^-$  state, the assignment of the multiplicity of this decay will constrain the  $J^\pi$  of the 239 keV state and hence the type of  $\beta$  decay to that state. The 50.5 keV  $\gamma$  ray is expected to be highly converted, with a large range of  $\sigma_{\text{tot}}$  values and consequently  $\beta$  feeding, depending on the multiplicity of the  $\gamma$  transition. Table III details the effect on the total intensity of the transition (with the sum of all observed transitions between levels equal to 100%),  $\beta$ -branching ratio to the 239 keV level and the  $\log ft$  of the multipolarity assignment of the 50.5 keV  $\gamma$  as  $E1$ ,  $M1$ ,  $E2$ , or  $M2$ .

As detailed in Table III, if the 50.5 keV transition is  $E1$ , the feeding to this level from above would exceed the amount deexciting this level, despite the fact that a  $9/2^+$  assignment would make this an allowed decay, which rules out  $E1$ . An assignment of  $E2$  (with  $J^\pi = 7/2^-$ ) would lead to very large apparent beta feeding to the 239 keV level of 35% and an apparent  $\log ft$  value of 5.0, which is far too low for a first forbidden transition. A  $M1$  assignment is the only one that gives a reasonable value for  $\beta$  feeding of 2.7(8)% and  $\log ft$  equal to 6.1 corresponding to a first forbidden transition. We therefore assign a  $J^\pi = (9/2^-)$  to this state.

Further evidence for the assignment of the 239-keV level as  $9/2^-$  comes from the level systematics of the lighter odd-mass Cd isotopes. In the cases of  $^{117,119,121,123}\text{Cd}$ , the first-excited state above the  $11/2^-$  isomer that decays to the isomer is a  $M1$  transition [4–7].

## 2. 384.1 and 643.7 keV levels

Within error bars the intensity of the  $\gamma$ s feeding the 384.1 keV level are equal to the intensity of the 384.1 keV  $\gamma$  making the observed  $\beta$  feeding to this state  $\approx 0$ . The level is fed by the ( $7/2^+$ ) 644-keV level and deexcites by a 384-keV  $\gamma$  which feeds the  $3/2^+$  ground state  $^{125}\text{Cd}$ . This is consistent with our proposed  $J^\pi$  of ( $5/2^+$ ), which would be a second forbidden  $\beta$  decay from the ( $9/2^+$ ) ground state.

The 643.7-keV level is strongly fed in the  $\beta$  decay of the  $9/2^+$  ground state of  $^{125}\text{Ag}$ , with an apparent feeding of 18.9(9)% and the corresponding  $\log ft = 5.2(1)$ . This strongly suggests an allowed  $\beta$  decay to this state. It decays strongly to the  $3/2^+$  ground state, and weakly to 239-keV ( $9/2^-$ ) state and the 384-keV ( $5/2^+$ ) state. The strong decay to the  $3/2^+$  state rules out  $11/2^+$  and  $9/2^+$ , leaving  $7/2^+$  as the likely  $J^\pi$  of this state. Further evidence for this assignment comes from studies of the neutron-rich  $^{121,123,125}\text{Cd}$  nuclei by Rejmund *et al.* [18]. In this study, they observed a 646 keV  $\gamma$  in the prompt (A and Z gated)  $\gamma$  spectrum. It is likely that this  $\gamma$  is the 643.8(2) keV  $\gamma$  observed in this work. This would establish the 643.8 keV transition as the lowest positive parity  $7/2^+$  to the  $3/2^+$  yrast transition. The other  $\gamma$ s observed in Ref. [18] were not observed in this work.

Figure 8 shows the  $\gamma$ - $\gamma$  coincidence spectrum generated by gating on the 643.8 keV  $\gamma$  transition. This shows that the ( $7/2^+$ ) 643.7 keV level is fed by  $\gamma$ s from the 1040.0, 1121.1, 1299.7, 1555.5, 1638.0, and 2120.4 keV levels (see inset of Fig. 8). The decays from these levels can be divided into two groups: (1) levels which feed the ( $5/2^+$ ) 384.1 and ( $7/2^+$ ) 643.7-keV levels and (2) levels which feed the 606.6 and

TABLE III. Effects of the assignment of possible multiplicities for the 50.5-keV transition in  $^{125}\text{Cd}$ . Column three reflects the total intensity of the transition (with the sum of all observed transitions between levels equal to 100%), i.e., it is not normalized to the 384 keV transition.

Mult.	$\sigma_{\text{tot}}$	$I_{\text{tot}}$	% $\beta$ feeding	log $ft$	$J^\pi$	$\beta$ transition
$E1$	1.14	5.8(1)%	−9.8(9)%		$9/2^+$	Allowed
$M1$	3.3	11.1(2)%	2.7(8)%	6.1(2)	$9/2^-$	First forbidden
$E2$	17.1	34.6(6)%	43.6(5)%	5.0(1)	$7/2^-$	First forbidden
$M2$	64.2	65.5(11)%	76.8(2)%	4.7(1)	$7/2^+$	Allowed ( $l$ forbidden)

( $7/2^+$ ) 643.7-keV levels. In the first group are the 1040.0 and 1121.1 keV levels. In the second group are the 1299.7, 1555.5, 1638.0 and 2120.4 keV levels. Of this second group, the levels at 1299.7, 1638.0 are only observed to feed the 643.7- and 606.6-keV levels and have an apparent log  $ft < 6$  (consistent with an allowed  $\beta$ -decay for the ( $9/2^+$ ) ground state), making them possible candidates for the ( $11/2^+$ ) yrast state.

### 3. 1121.1 keV level

Like the above 643 keV level, the 1121.1 keV level is strongly fed in the  $\beta$  decay of the ( $9/2^+$ ) ground state in  $^{125}\text{Ag}$ , with an apparent  $\beta$  feeding of 12.1(11)% with a log  $ft$  of 5.3(1), suggesting an allowed decay to this state with possible  $J^\pi$  of  $7/2^+$ ,  $9/2^+$  and  $11/2^+$ . The state strongly decays to the ( $9/2^-$ ) 239 and  $11/2^-$  189-keV states and has weaker decays to the ( $5/2^+$ ) 384 and ( $7^+$ ) 644-keV states. The spin of  $7/2^+$  is excluded because the level does not have a branch to the  $3/2^+$  ground state (which would be  $E2$ ). Spin equal to  $11/2^+$  is also excluded as the transition to the ( $5/2^+$ ) 384 keV state would be  $M3$ . We therefore assign this level as ( $9/2^+$ ).

### 4. 873.5, 986.9, 1051.2, and 1164.6 keV levels

The four levels at energies of 873.5, 986.9, 1051.2, and 1164.6 keV have been observed to decay to the ( $9/2^-$ ) 239.1-

keV level, with no observed decay into the positive-parity states at 643.7 ( $7/2^+$ ), 384.1 ( $5/2^+$ ) or 0.0 ( $3/2^+$ ) keV. The apparent log  $fts$  to these levels are all  $> 6$ , which is consistent with a first forbidden decay from the ( $9/2^+$ ) ground state of  $^{125}\text{Ag}$  to negative-parity states. Of these states, only the 1164.6 level has been observed to decay to the  $11/2^-$  188.5 keV isomer. The transition from the 986.9-keV level to the 188.5 keV level is not observed with a lower limit of  $< 0.3\%$  (normalized to the 384.1 transition). Low-intensity transitions from the 873.5- and 1051.2-keV states of 685.0 and 862.8 keV, respectively, to the  $11/2^-$  isomer would not be observed in the singles spectrum because of contamination from relatively large peaks resulting from the decay of  $^{125}\text{Cd}$  at 683.6 and 859.7 keV [10]. There is a ( $15/2^-$ ) level reported in Ref. [13] at  $x + 719.7(2)$  keV, where  $x$  is the energy of the  $11/2^-$  isomer. With our value of 188.5(2), this puts the ( $15/2^-$ ) level at 931.8(3) keV. Based on the closeness of energies to the ( $15/2^-$ ) level, the 873.5- and 986.9-keV levels are possible candidates for  $7/2^-$  and  $11/2^-$  core coupled levels.

### B. Decay of the ( $1/2^-$ ) isomer of $^{125}\text{Ag}$

The 352.6-keV  $\gamma$  transition is not connected via  $\gamma$ - $\gamma$  coincidence to any transitions we have assigned to the decay of the ( $9/2^+$ ) ground state of  $^{125}\text{Ag}$  (although the decay schemes of the two isomers are connected by the 190.5 keV transition—

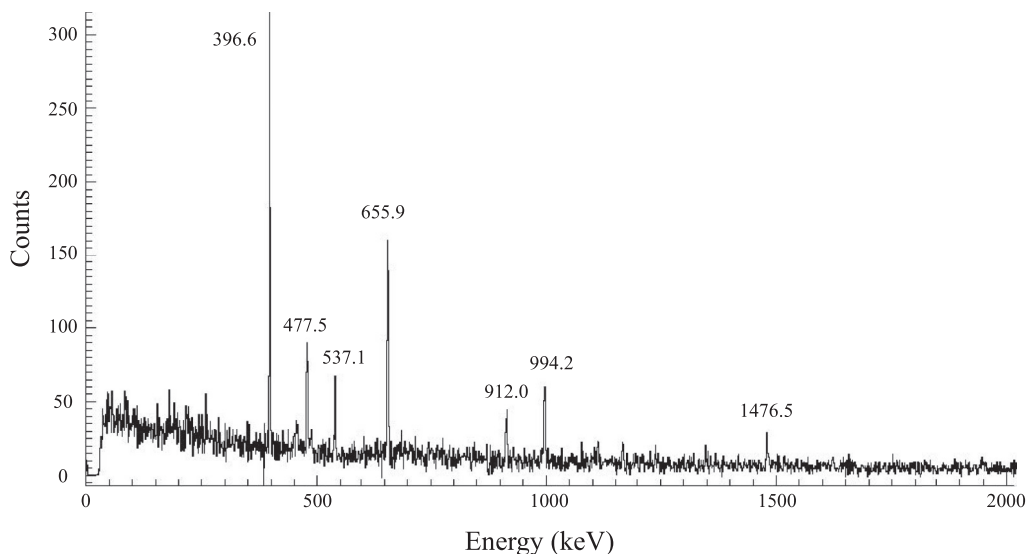


FIG. 8.  $\beta$ -gated  $\gamma$ -ray spectrum coincident with the 643.8-keV transition. Prominent  $\gamma$  peaks that are included in our proposed decay scheme of  $^{125}\text{Ag}$  are labeled.

TABLE IV. List of  $\gamma$  rays resulting from the beta decay of  $^{125m}\text{Ag}$  to levels in  $^{125}\text{Cd}$ . The intensities in columns two and four are normalized to the 100% 352-keV transition. The  $I_{\text{tot}}$  intensities in column four are the total transition strength ( $I_{\gamma} + I_{\text{conversion electron}}$ ). Gamma intensities are based on (a) singles, or (b) coincidence relationships. The \* symbol denotes that the  $\gamma$  was not placed in the level scheme. Contaminants from the  $\beta$  decay of  $^{125}\text{Cd}$  are marked with the symbol \*\*.

$E_{\gamma}$ (keV)	$I_{\gamma}$ (%)	$\alpha_{\text{tot}}$	$I_{\text{tot}}$ (%)	$E_i$	$E_f$	Mult.	Coincident $\gamma$ rays
190.5(4)	10.5(9) <sup>b</sup>	0.152	11.7(7)	574.8	384.1	(E2)	193*, 334*, 384, 606**, 737**, 1173**
222.0(3)	7.1(11) <sup>b</sup>		7.4(11)	574.7	352.6		353
352.6(1)	100 <sup>a</sup>	0.018	100	352.6	0.0	(M1, E2)	222, 1023, 1079, 1167, 1725, 1781, 1785 1888, 1940, 2047, 2805, 2825, 2969
384.1	11.7(7) <sup>b</sup>	0.0041	11.7(7)	384.1	0.0	[E1]	191
574.8(2)	19.7(9) <sup>a</sup>		19.0(9)	574.7	0.0		
1022.7(3)	2.8(9) <sup>b</sup>		2.7(9)	1375.3	352.6		353
1079.2(4)	3.2(8) <sup>b</sup>		3.1(8)	1431.7	352.6		353
1166.7(4)	6.1(11) <sup>b</sup>		6.0(10)	1519.3	352.6		353
1725.2(4)	5.6(12) <sup>b</sup>		5.5(12)	2077.8	352.6		353
1780.9(4)	13.9(16) <sup>b</sup>		13.7(16)	2133.7	352.6		353
1795.4(3)	2.9(10) <sup>b</sup>		2.8(10)	2148.0	352.6		353
1888.0(3)	5.3(12) <sup>b</sup>		5.2(12)	2240.6	352.6		353
1940.4(3)	7.4(15) <sup>b</sup>		7.2(15)	2293.0	352.6		353
2046.6(5)	7.2(15) <sup>b</sup>		7.1(15)	2399.2	352.6		353
2133.8(3)	25.7(18) <sup>a</sup>		25.3(18)	2133.7	0.0		
2804.7(4)	18(2) <sup>b</sup>		18(2)	3157.3	352.6		353
2825.0(3)	4.2(10) <sup>b</sup>		4.1(10)	3177.6	352.6		353
2968.7(5)	6.2(12) <sup>b</sup>		6.1(11)	3321.3	352.6		353
3157.5(4)	3.8(5) <sup>a</sup>		3.7(5)	3157.3	0.0		

see the 574.8 keV level section below). The energy of this  $\gamma$  matches well with the reported 352.7-keV  $\gamma$  assigned to the decay of  $^{125m}\text{Ag}$  from Ref. [23]. We therefore assign this transition and those in coincidence with it to the  $\beta$  decay of the  $(1/2^-)$  isomer. Table IV lists the transitions assigned to this decay along with their intensities, initial and final states, assigned multiplicities, and coincidence relationships. Tran-

sitions and levels that require further explanation are listed in the following sections by level.

Table V lists the levels in  $^{125}\text{Cd}$  populated in this decay. As noted previously, the calculated  $\log ft$  values are based on the apparent  $\beta$  feeding and should be considered as lower limits and direct decays to the ground state and isomer are assigned an upper limit based on the  $J^{\pi}$  values of the initial and final levels. The direct  $\beta$  decay of the  $(1/2^-)$  ground state to the  $3/2^+$  ground state of  $^{125}\text{Cd}$  would be a first forbidden  $\beta$  decay with a corresponding  $\log ft > 6$ , resulting in a branching ratio of  $< 4\%$ . A direct  $\beta$  decay to the  $11/2^-$  isomer in  $^{125}\text{Cd}$  would require a fourth forbidden  $\beta$  decay and therefore have a branching ratio of  $\approx 0$ . The resulting decay scheme is shown in Figs. 6 and 7.

TABLE V. Levels in  $^{125}\text{Cd}$  populated by the  $\beta$  decay of  $1/2^-$   $^{125m}\text{Ag}$ .

Level (keV)	$\beta$ %	$\log ft$
0.0	$< 4$	$> 6$
188.5(2)	0	
352.6(1)	7.6(28)	5.6(3)
574.8(3)	22.7(9)	5.1(2)
1375.3(3)	1.6(5)	6.1(2)
1431.7(4)	1.9(5)	6.0(2)
1519.3(4)	3.5(6)	5.7(2)
2077.8(4)	3.3(7)	5.6(2)
2133.7(4)	23.0(9)	4.7(2)
2148.0(3)	1.7(6)	5.8(2)
2240.6(3)	3.1(7)	5.5(2)
2293.0(3)	4.3(8)	5.4(2)
2399.2(5)	4.2(9)	5.4(2)
3157.3(4)	12.7(11)	4.6(2)
3177.6(3)	2.4(6)	5.4(2)
3321.3(5)	3.6(7)	5.1(2)
$> 4621$	4.6(12)	

### 1. 574.8 keV level

The 574.8 keV level is strongly fed by the  $\beta$  decay of the  $(1/2^-)$  isomer of  $^{125}\text{Ag}$  with an apparent  $\log ft$  of 5.1, which is consistent with an allowed  $\beta$  decay. It then decays to the  $3/2^+$  ground state, the  $(1/2^+)$  352.6-keV, and  $(5/2^+)$  384.1-keV states. This is suggestive of a  $(3/2^-)$  assignment for this level, however, a mechanism for lowering a  $(3/2^-)$  to that energy is unknown to the best of our knowledge. However, systematics would suggest an assignment of  $(3/2^+)$  to this state resulting from a first forbidden decay. It is likely that the actual  $\log ft$  to this level is much higher than the apparent value of 5.1 due to unobserved transitions to the 574.8 level from higher-lying states. Note that the statistics from the decay of the  $(1/2^-)$  beta decay are much lower than those from decay of the  $(9/2^-)$  ground state.

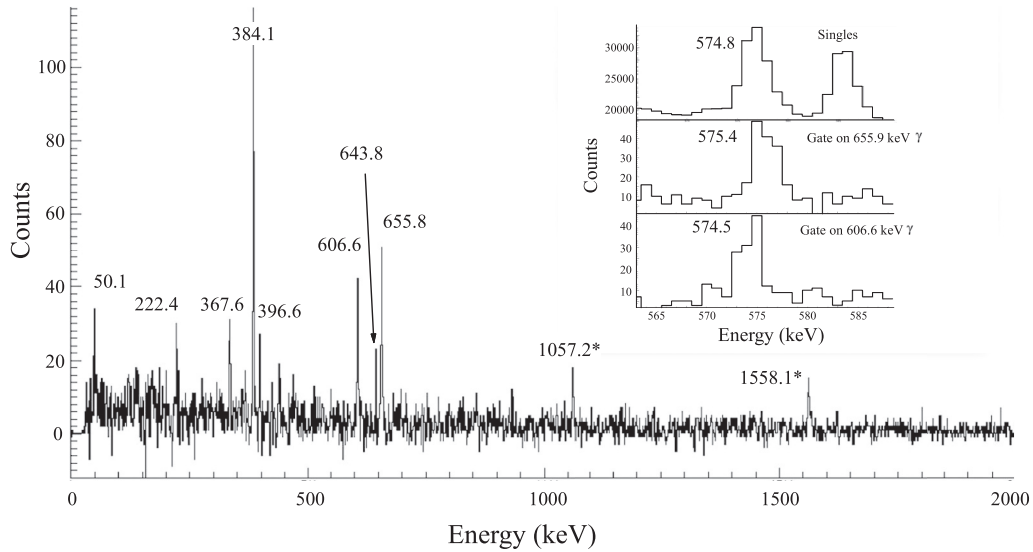


FIG. 9.  $\beta$ -gated  $\gamma$ -ray spectrum coincident with the 575-keV multiplet. Prominent  $\gamma$  peaks are labeled. The inset shows the energy of the peak in the singles spectrum (top), in coincidence 606.6-keV  $\gamma$  (middle), and the 655.9-keV  $\gamma$  (bottom), with the fitted peak energy displayed.

We assign three  $\gamma$ s in this work that have energies close to 575 keV: (1) 574.5 keV deexciting the 1180.8 level to the 606.6-keV level, (2) 575.4 keV deexciting the 1615.4 level to the 1040.0-keV level, and (3) 574.8 keV deexciting the 574.8-keV level to the ground state. For the first two transitions, the energy and intensity were determined via coincident  $\gamma$  gates on the 606.6- and 655.8-keV  $\gamma$ s, respectively. A comparison of these two intensity values to the 575 peak in the singles spectra shows that there is an excess of counts which indicates a third peak. The energy of this peak at 574.8 keV and its intensity were determined from the  $\beta$ -gated  $\gamma$  spectrum after subtracting out the contributions of the first two transitions from the multiplet. The spectrum obtained by gating on the

575-keV multiplet is shown in Fig. 9, with a closeup of the three 574.8-, 574.5-, and 575.4-keV  $\gamma$ s that make up the multiplet in the singles spectrum and gated on the 606.6- and 655.9-keV  $\gamma$ s, respectively.

The 190.5 keV transition decays from the 754.8 keV level to the 384.1 keV level and connects the levels fed by the  $(1/2^-)$  isomer with those fed by the  $(9/2^-)$  ground state. In our data there is a significant amount of  $\gamma$ s from the decay of  $^{125}\text{Cd}$ , including the known 191.88(15)-keV transition [10]. The  $\gamma$ - $\gamma$  coincident gate on the 191-keV multiplet is shown in Fig. 10. The prominent peaks in coincidence are the 384.1-keV (from  $^{125}\text{Ag}$ ) and the 736.7 and 1173.2-keV transitions (from  $^{125}\text{Cd}$ ). Gating on the 736.7-keV  $\gamma$  gives a peak at

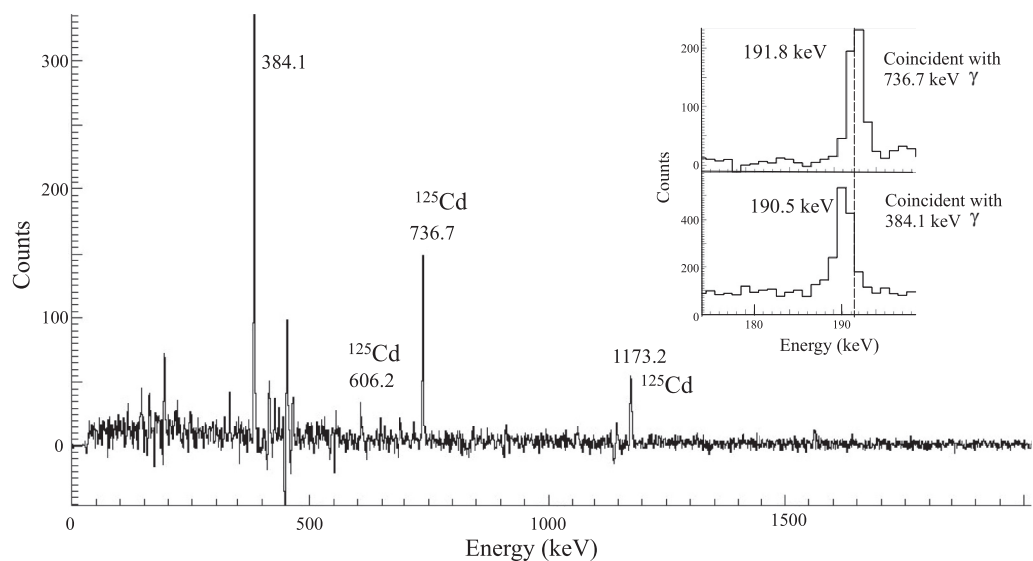


FIG. 10.  $\beta$ -gated  $\gamma$ -ray spectrum coincident with the 190.5-keV transition. Prominent  $\gamma$  peaks are labeled. There is significant contamination in this peak from the 191.88(15)-keV  $\gamma$  resulting from the  $\beta$  decay of  $^{125m}\text{Cd}$ . The inset shows the energy of the peak in coincidence with the  $^{125}\text{Ag}$  384.1-keV  $\gamma$  (top), and the 736.7-keV  $\gamma$  (bottom) from  $^{125}\text{Cd}$ . A dashed line was added to the inset to guide the eye.

TABLE VI. Observed  $\gamma$  rays in this work from the  $\beta$  decay of  $^{124}\text{Cd}$ .

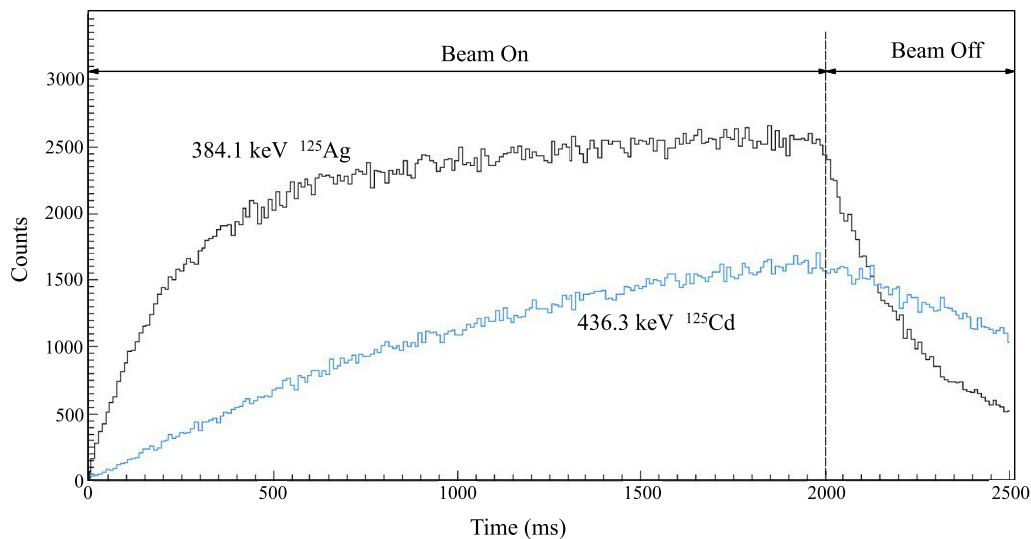
$E_\gamma$ (keV)	$I_\gamma$	$\alpha_{\text{tot}}$	$I_{\text{tot}}$	$E_i$	$E_f$	Mult.	Coin. $\gamma$ rays
62.2(3)	28(17)	0.664	47(29)	62.3	0.0	E1	142.9, 179.3
142.9(3)	10(4)	0.063	11(4)	205.2	62.3	E1	62.3
179.4(3)	42(12)	0.033	43(12)	241.6	62.3	E1	62.3
241.7(4)	12(3)	0.07	13(3)	241.6	0.0	E2	

TABLE VII.  $\beta$ -delayed neutron emission results from  $^{125}\text{Ag}$  and  $^{125m}\text{Ag}$ .

Nuclide	$J\pi$	Allowed $\beta$ decays	Final state ( $^{124}\text{Cd}$ )	$\Delta\ell$	$\beta$ -n branching
$^{125}\text{Ag}$	$(9/2^+)$	$7/2^+, 9/2^+, 11/2^+$	$5^-, 1846$ keV	0, 1, 2	0.56(5)%
			$4^+, 1385.2$ keV	0, 1	0.59(10)%
			$2^+, 613.0$ keV	1, 2, 3	0
			$0^+$ , ground state	3, 4, 5	0
$^{125m}\text{Ag}$	$(1/2^-)$	$1/2^-, 3/2^-$	$5^-, 1846$ keV	3, 4	0
			$4^+, 1385.2$ keV	2, 3	0
			$2^+, 613.0$ keV	0, 1	1.5(2)%
			$0^+$ , ground state	0, 1	3.1(10)%

TABLE VIII. Comparison of experimental and theoretical  $\beta$ -delayed neutron probabilities for the odd-mass neutron-rich Cd isotopes.

Nuclide	Theory [35]	Theory [36]	Lit. value (expt.)	This work
$^{120}\text{Ag}$	0	0.5%	<0.003% [37]	
$^{121}\text{Ag}$	0	0.7%		
$^{122}\text{Ag}$	0	0.6%	0.186(10)% [37]	
$^{123}\text{Ag}$	7%	0.9%	0.55(9)% [37]	
$^{124}\text{Ag}$	10%	0.7%	1.3(9)% [38]	
$^{125}\text{Ag}$	4%	1.1%	11.8(10)% [20], 2.2(11)% [21]	4.6(12)% ( $^{125m}\text{Ag}$ ) 1.2(2)% ( $^{125}\text{Ag}$ )
$^{126}\text{Ag}$	4%	1.0%	13.7(11)% [20]	
$^{127}\text{Ag}$	7%	1.9%	14.6(15)% [20]	
$^{128}\text{Ag}$	9%	1.8%	20(5)% [20]	
$^{129}\text{Ag}$	10%	13.3%	<20% [20]	

FIG. 11. Timing spectrum of 384.1-keV transition arising from the  $\beta$  decay of  $^{125}\text{Ag}$  compared with the 436.3-keV transition from the  $\beta$  decay of  $^{125}\text{Cd}$ .

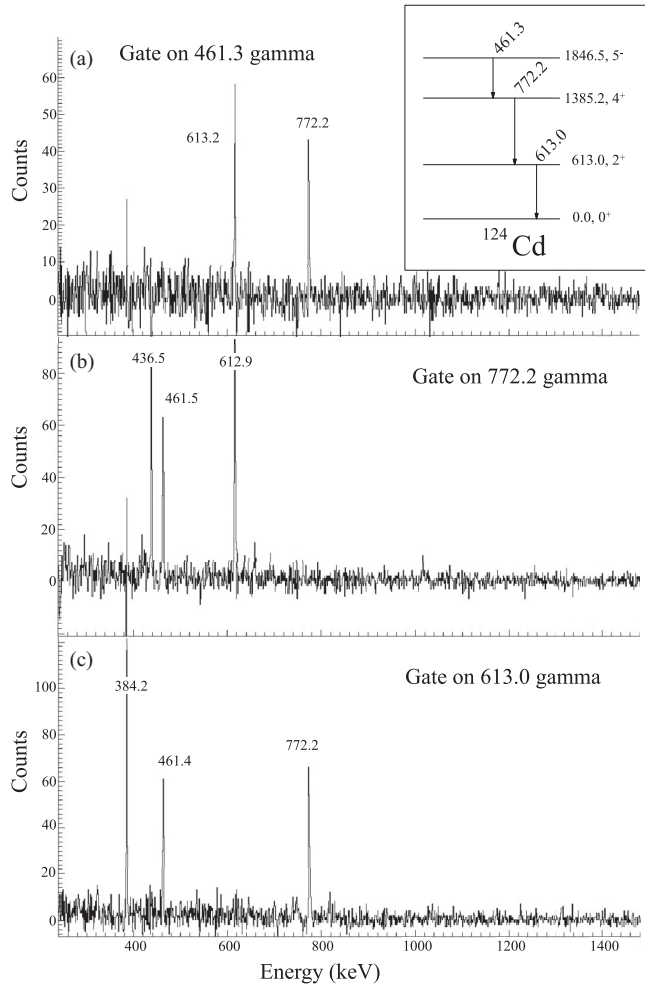


FIG. 12. Gamma spectra gated on the known  $\gamma$  rays in  $^{124}\text{Cd}$  arising from the  $\beta$ -delayed neutron emission of  $^{125}\text{Ag}$ .

191.8 keV, which agrees well with the literature value [10], and gating on the 384.1-keV peak yields a peak at 190.5 keV (see inset of Fig. 10).

### C. Half-lives

The measurements of the half-lives of the ground state and isomer in  $^{125}\text{Ag}$  were done by measuring the apparent half-life of each  $\gamma$  ray with time equal zero defined as when the tape moved the sample to the front of the detectors. As detailed above, the  $A = 125$  beam was on for two seconds, then turned off for 500 ms to allow measurements of the half-lives of the ground state and isomer in  $^{125}\text{Ag}$  (and  $^{125}\text{Cd}$ ). This was done by measuring the apparent half-life of the most intense  $\gamma$  rays of each starting when the beam was tuned off. The measured half-life ( $T_{1/2}^{\text{tot}}$ ) is a combination of the  $\beta$  decay  $T_{1/2}^{\beta}$  and the  $\gamma$ -ray decay  $T_{1/2}^{\gamma}$ , where it was assumed  $T_{1/2}^{\gamma} \ll T_{1/2}^{\beta}$ . This is shown in Fig. 11 for the 384.1 keV  $\gamma$  transition from the  $\beta$  decay of  $^{125}\text{Ag}$  and the 436.3 keV  $\gamma$  transition from the  $\beta$  decay of  $^{125}\text{Cd}$ . In Fig. 11, the grow-in (beam on) and decay (beam off) of both nuclei is observed. In this figure, time equal zero corresponds to the tape movement. Note that  $^{125}\text{Cd}$  is

produced both directly and as the  $\beta$  daughter, making the time spectrum more complicated than for the  $^{125}\text{Ag}$  activity, which is only produced directly.

For the ground-state  $\beta$  decay of  $^{125}\text{Ag}$ , the half-life was obtained from the weighted average of the largest gamma peaks in its decay. The  $\gamma$ s used were the 50.5-, 384.1-, 643.8-, and 606.6-keV transitions with measured  $T_{1/2}$  values of 176.1(49), 176.4(50), 173.5(80), and 174(15), respectively, resulting in a weighted average of 176(3) ms. For the isomer of  $^{125}\text{Ag}$ , the half-life was obtained from the 352.6-keV transition to be 159(21) ms.

### D. $\beta$ -delayed neutron emission

Known  $\gamma$  rays from levels in  $^{124}\text{Cd}$  are present in the data with the assignment made by  $\gamma$ - $\gamma$  coincidences. The available energy for  $\beta$ -decay into neutron unbound states  $Q_n^{\beta}$  is 4110(430) keV [24] out of a total  $Q_{\beta}$  of 8830(430) keV. The lowest energy levels in  $^{124}\text{Cd}$  above the  $0^+$  ground state are the  $2^+$  613.0 keV,  $4^+$  1385.2 keV,  $2^+$  1427.2,  $0^+$  1573.1, and the ( $5^-$ ) 1846.5 keV states [33]. Gammas from the 613.0, 1385.2, and 1846.5 keV states have been observed with the expected coincidence relationships. Figures 12(a)–12(c) show the coincidence spectra gated on the 461.3 keV, 772.2 keV, and 613.0 keV  $\gamma$  rays, respectively. In all three spectra, the expected  $\gamma$  rays are all observed. In addition, the gate on the 772-keV  $\gamma$  has a peak at 436.5 keV, which results from coincidence with the tail of the unresolved 774.5 keV  $\gamma$  arising from the  $\beta$  decay of  $^{125}\text{Cd}$  [10]. The 384 keV peak in the 613.0 keV gated spectrum arises from the tail of the unresolved 615.1 keV  $\gamma$  from  $^{125}\text{Ag}$ .

We also observed  $\gamma$ s with energies of 62.2(3), 142.9(3), 179.4(3), and 241.7(4) keV, which match well with the known 62.2(1), 143.0(2), 179.6(1), and 242.0(3) keV  $\gamma$ s [34] arising from the  $\beta$  decay of  $^{124}\text{Cd}$ . These are listed in Table VI. Fig. 13 shows the  $\gamma$  coincidence spectrum gated on the 62-keV  $\gamma$ . The expected 179- and 143-keV  $\gamma$ s are observed in the spectrum. The 36.5 keV line is absent because it is below the energy threshold. The inset of the figure shows the decay scheme from Ref. [34].

Neutron emission to states in  $^{124}\text{Cd}$  are expected to occur predominately from excited levels in  $^{125}\text{Cd}$  with similar  $J^{\pi}$  values. These neutron-emitting states are populated primarily by allowed (and to a lesser extent first forbidden)  $\beta$  decays of  $^{125}\text{Ag}$ . These neutron unbound states will then decay by neutron emission to states in  $^{124}\text{Cd}$  requiring the smallest change in angular momentum—primarily  $\Delta\ell = 0$ . Therefore, we assign those  $\beta$ -delayed neutrons to the ( $4^+$ ) 1385.2 and ( $5^-$ ) 1846.5 keV levels in  $^{124}\text{Cd}$  as arising from the  $\beta$ -delayed neutron emission of the ( $9/2^+$ ) ground state and the delayed neutrons populating the  $2^+$  613.0 keV and  $0^+$   $^{124}\text{Cd}$  ground state as arising from the ( $1/2^-$ ) isomer of  $^{125}\text{Ag}$ . This is detailed in Table VII, showing  $\ell = 0$  delayed neutron emission to the  $5^-$  and  $4^+$   $^{124}\text{Cd}$  states from the ( $9/2^+$ ) ground state and emission to the  $2^+$  and  $0^+$   $^{124}\text{Cd}$  states from the ( $1/2^-$ ) isomeric state. Determining the delayed-neutron branching ratio to the excited states in  $^{124}\text{Cd}$  is a straightforward ratio compared with other observed  $\gamma$ s from  $^{125}\text{Ag}$ . The branching ratio to the ground state of  $^{124}\text{Cd}$  was determined by

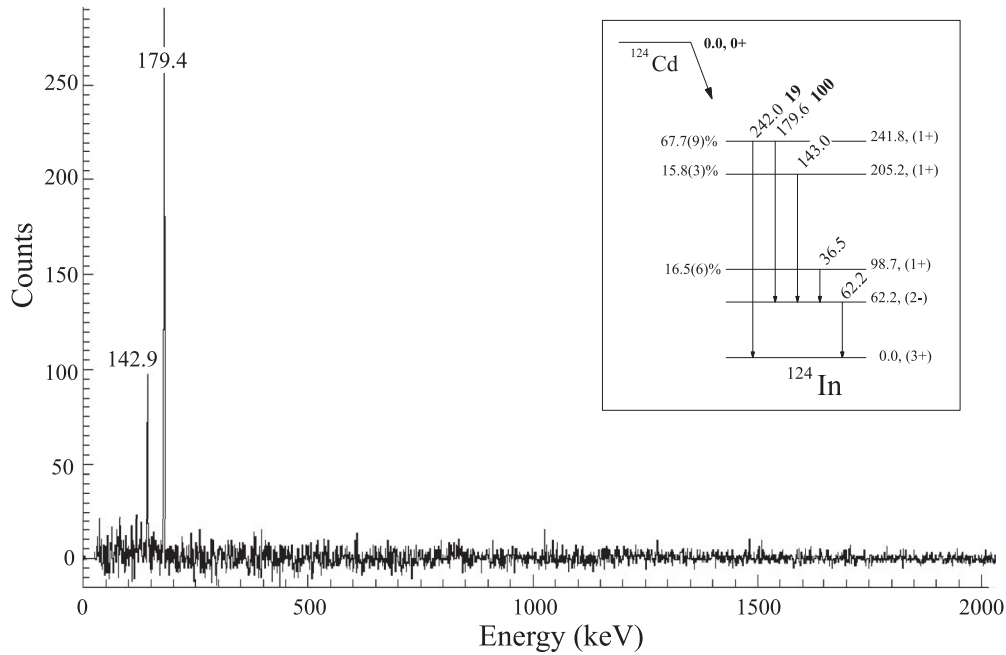


FIG. 13.  $\beta$ -gated  $\gamma$ -ray spectrum coincident with the 62.2-keV  $\gamma$  ray arising from the  $\beta$  decay of  $^{124}\text{Cd}$ . The inset of the figure shows the decay scheme from Ref. [34].

subtracting the relative amount of  $^{124}\text{Cd}$  beta decay determined by the 179 keV  $\gamma$ s from  $\beta$  decay of  $^{124}\text{Cd}$  to the observed 613 keV  $\gamma$  in  $^{124}\text{Cd}$  from  $\beta$ -delayed neutron decay of  $^{125}\text{Ag}$  (see Fig. 12).

This results in a branching ratio for the  $(9/2^+)$   $^{125}\text{Ag}$  ground state of 1.2(2)% [0.56(5)% to the 1846 keV level and 0.59(10)% to the 1385 keV level], and 4.6(12)% [1.5(2)% to the 613 keV level and 3.1(10)% to the ground state] for the  $(1/2^-)$  isomer (see table VII). The assigned value of the  $\beta$ - $n$

branching to the  $^{124}\text{Cd}$  ground state should be considered as a lower limit because the beta branching ratios to the 241.8-keV (<67.7%) and 205.2-keV level (<15.8%) are considered to be upper limits [34] due to the pandemonium effect [32]. The resulting decay scheme for  $\beta$ -delayed neutron emission from  $^{125,125m}\text{Ag}$  is shown in Fig. 14.

A comparison of the  $\beta$ - $n$  branching ratios calculated by Moller *et al.* [35] and Marketin *et al.* [36] versus experimental literature values for the neutron-rich odd-mass is shown

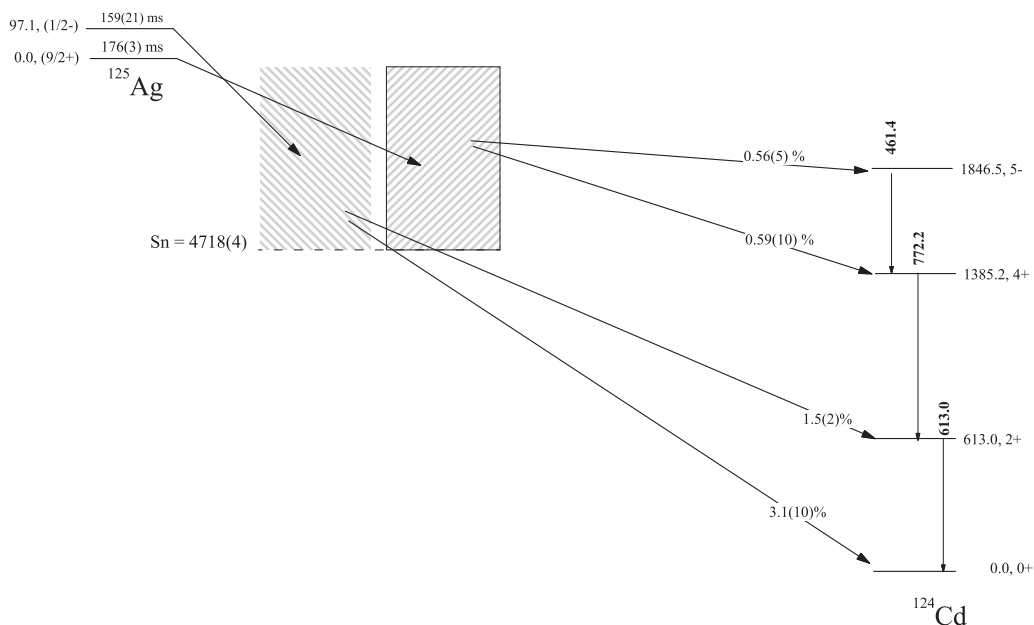


FIG. 14. Proposed partial decay scheme for  $\beta$ -delayed neutron emission from  $^{125,125m}\text{Ag}$ .



in Table VIII. Our experimental values of 1.2(2)% for the  $9/2^+$   $^{125}\text{Ag}$  and 4.6(10)% for the  $1/2^-$   $^{125m}\text{Ag}$  are significantly lower than the previously reported value of 11.8(10)% [20] and matches somewhat with the value of 2.2(11)% [21], which is a combination of decays from the ground state and isomer.

In conclusion, we have investigated the  $\beta$  decay of  $^{125}\text{Ag}$ . We have found evidence for  $\beta$  decay and  $\beta$ -delayed neutron emission from both the ( $9/2^+$ ) ground state and the ( $1/2^-$ ) isomer of  $^{125}\text{Ag}$ . The resulting partial decay scheme of  $^{125m}\text{Ag}$  consists of 16  $\gamma$ s from 14 levels in the  $\beta$  daughter, while the partial decay scheme of the ground state of  $^{125}\text{Ag}$  consists of 72  $\gamma$ s from 47 levels. In both the isomer and ground state, evidence for  $\beta$ -delayed neutron emission was observed, with

the resulting branching ratios of 4.6(12)% for the isomer, and 1.2(2)% for the ground state.

#### ACKNOWLEDGMENTS

This work has been supported by the U. S. Department of Energy, Office of Nuclear Physics under contracts DE-AC02-05CH11231, DOE-AC05-00OR22725, DE-FG05-88ER40407, DE-FG02-96ER40983, DE-FG02-96ER41006, DE-SC00144448 and the National Nuclear Security Administration (NNSA) under the Stewardship Science Academic Alliances program through U.S. Department of Energy (DOE) Cooperative Agreements No. DE-FG52-08NA28552 and No. DE-NA0002132.

- 
- [1] T. Kracikova, I. Prochazka, Z. Hons, M. Fiser, and A. Kuklik, *Czech. J. Phys. B* **27**, 1099 (1977).
- [2] B. Fogelberg, Y. Zongyuan, B. Ekstrom, E. Lund, K. Aleklett, and L. Sihver, *Z. Phys. A* **337**, 251 (1990).
- [3] W. Bruchle and G. Herrmann, *Radiochim. Acta* **30**, 1 (1982).
- [4] B. Fogelberg, Y. Kawase, J. McDonald, and A. Backlin, *Nucl. Phys. A* **267**, 317 (1976).
- [5] B. Fogelberg and P. Hoff, *Nucl. Phys. A* **391**, 445 (1982).
- [6] H. Huck, A. Jech, G. Marti, M. L. Perez, J. J. Rossi, and H. M. Sofia, *Phys. Rev. C* **40**, 1384 (1989).
- [7] Y. Kawase, B. Fogelberg, J. McDonald, and A. Bäcklin, *Nucl. Phys. A* **241**, 237 (1975).
- [8] G. H. Fuller, *J. Phys. Chem. Ref. Data* **5**, 835 (1976).
- [9] H. Penttilä, J. Aysto, K. Eskola, Z. Janas, P. P. Jauho, A. Jokinen, M. E. Leino, J. M. Parmonen, and P. Taskinen, *Z. Phys. A: Hadrons Nucl.* **338**, 291 (1991).
- [10] H. Huck, A. Jech, G. Marti, M. L. Perez, J. J. Rossi, and H. M. Sofia, *Phys. Rev. C* **39**, 997 (1989).
- [11] A. Kankainen *et al.*, *Phys. Rev. C* **87**, 024307 (2013).
- [12] D. Lascar *et al.*, *Phys. Rev. C* **96**, 044323 (2017).
- [13] N. Hoteling *et al.*, *Phys. Rev. C* **76**, 044324 (2007).
- [14] Ch. Lorenz *et al.*, *Phys. Rev. C* **99**, 044310 (2019).
- [15] J. Taprogge *et al.*, *Phys. Lett. B* **738**, 223 (2014).
- [16] A. Scherillo, J. Genevey, J. A. Pinston, A. Covello, H. Faust, A. Gargano, R. Orlandi, G. S. Simpson, I. Tsekhanovich, and N. Warr, *Phys. Rev. C* **70**, 054318 (2004).
- [17] G. S. Simpson, A. Scherillo, J. Genevey, R. Orlandi, J. A. Pinston, I. S. Tsekhanovich, N. Warr, A. Covello, and A. Gargano, *J. Phys.: Conf. Ser.* **267**, 012031 (2011).
- [18] M. Rejmund, A. Navin, S. Bhattacharyya, M. Caamano, E. Clement, O. Delaune, F. Farget, G. de France, B. Jacquot, and A. Lemasson, *Phys. Rev. C* **93**, 024312 (2016).
- [19] V. N. Fedoseyev *et al.*, *Z. Phys. A: Hadrons Nucl.* **353**, 9 (1995).
- [20] K. I. Smith, Ph.D. thesis, University of Notre Dame, 2014 (unpublished).
- [21] O. Hall *et al.*, *Phys. Lett. B* **816**, 136266 (2021).
- [22] G. Lorusso *et al.*, *Phys. Rev. Lett.* **114**, 192501 (2015).
- [23] Z. Q. Chen *et al.*, *Phys. Rev. Lett.* **122**, 212502 (2019).
- [24] W. J. Huang, M. Wang, F. G. Kondev, G. Audi, and S. Naimi, *Chin. Phys. C* **45**, 030002 (2021).
- [25] B. E. Tomlin, P. F. Mantica, and W. B. Walters, *Eur. Phys. J. Spec. Top.* **150**, 183 (2007).
- [26] D. W. Stracener, in *Proceedings of the Sixteenth International Conference on the Application of Accelerators in Research and Industry*, edited by J. L. Duggan and I. L. Morgan, AIP Conf. Proc. No. 576 (AIP Press, New York, 2000), pp. 257–260.
- [27] J. R. Beene *et al.*, *J. Phys. G* **38**, 024002 (2011).
- [28] W. A. Peters *et al.*, *Nucl. Instrum. Methods Phys. Res., Sect. A* **836**, 122 (2016).
- [29] Y. Zhao, Ph.D. thesis, Tokyo Metropolitan University, 1996.
- [30] <http://www.xia.com/>.
- [31] T. Kibédi, T. W. Burrows, M. B. Trzhaskovskaya, P. M. Davidson, and C. W. Nestor, Jr., *Nucl. Instrum. Methods Phys. Res., Sect. A* **589**, 202 (2008).
- [32] J. C. Hardy, L. C. Carraz, B. Jonson, and P. G. Hansen, *Phys. Lett. B* **71**, 307 (1977).
- [33] J. C. Batchelder *et al.*, *Phys. Rev. C* **89**, 054321 (2014).
- [34] J. C. Batchelder *et al.*, *Phys. Rev. C* **94**, 024317 (2016).
- [35] P. Möller, M. R. Mumpower, T. Kawano, and W. D. Myers, *At. Data Nucl. Data Tables* **125**, 1 (2019).
- [36] T. Marketin, L. Huther, and G. Martínez-Pinedo, *Phys. Rev. C* **93**, 025805 (2016).
- [37] P. L. Reeder, R. A. Warner, and R. L. Gill, *Phys. Rev. C* **27**, 3002 (1983).
- [38] F. Montes *et al.*, *Phys. Rev. C* **73**, 035801 (2006).